2

MEMS Based on Thin Ferroelectric Layers

Igor L. Baginsky and Edward G. Kostsov
Institute of Automation and Electrometry,
Russian Academy of Sciences,
Russia

1. Introduction

Micro-Electro-Mechanical Systems (MEMS) are devices that display the most intense development in modern microelectronics (Kostsov, 2009).

The main challenge of microelectromechanics is the design of unique micromechanical structures for various purposes. This research direction is based on achievements of advanced microelectronic technologies and inherits the basic advantages of electronic microchips: high reliability and reproducilbility of characteristics, low cost, and large scales of applications (Esashi & Ono, 2005). The essence of micromechanics implies that advanced microelectronic technologies, for instance, deep etching of silicon (or silicon-on-insulator (SOI)) make it possible to create integrated circuits (ICs) simultaneously with micromechanical structures with unique parameters (determined by their microscopic or nanoscopic sizes, with the transported mass being 10^{-4} to 10^{-18} g) controlled by electronic circuits.

The most important feature of MEMS is the precision fabrication of moving elements of mechanical structures (earlier inaccessible in mechanics) and their unification in one technological cycle with controlling and processing electronic elements created on the basis of CMOS technology.

MEMS applications include the following areas (Kostsov, 2009):

- microoptoelectromechanics (displays, adaptive optics, optical microswitches, fast-response scanners for cornea inspection, diffraction gratings with an electrically tunable step, controlled two- and three-dimensional arrays of micromirrors, etc.);
- high frequency (HF) devices (HF switches, tunable filters and antennas, phased antenna array, etc.);
- displacement meters (gyroscopes, highly sensitive two- and three-axial accelerometers with high resolution, which offer principally new possibilities for a large class of electronic devices);
- sensors of vibrations, pressures, velocities, and mechanical stresses; microphones (there are millions of them in cellular phones). Back in 2004, Intel started to deliver RF front-end assemblies fabricated by the MEMS technology for cellular phones. They integrate approximately 40 passive elements, which allows the producer to save up to two thirds of space in the phone casing;
- wide range of devices for working with microvolumes of liquids and for applications in biology, biochips, biosensors, chemical testing, creation of a new class of chemical sensors, etc.;
- microactuators and nanopositioners; microgenerators of energy.

Many experts think that the telecommunications market is one of the promising areas of MEMS implementation, including the technologies related to optical switches for fiber-optical telecommunications systems.
It becomes obvious that none of the fields of modern electronic engineering will avoid the touch of the new industrial revolution.
The basic component of most micromechanical devices is the energy converter, namely, micromotor (or microactuator). Therefore, the main attention in this work is paid to the analysis of the operation of new micromotor proposed by us, the examples of the micromotor application in MEMS devices are presented at the end of the chapter.
There are electromagnetic, electrothermal, piezoelectric and electrostatic effects among the variety of physical principles basic for these converters.
Presently, there are two common kinds of the motors (the devices that convert electrical energy into the mechanical motion): induction motors (IM) and electrostatic motor (EM). Classic electrostatic motors are not widely used mainly because it is necessary to use high operating voltage to achieve the specific energy output comparable with IM motors. At the same time, the specific energy output of the IM decreases as their power becomes small, and this decrease starting from power of 10-100 mW makes induction micromotors ineffective.
The advantages of the capacitance (EM) machines over IM machines in the low power domain can be attributed to the main difference between the electric and magnetic phenomena: the existence of electric monopoles and the absence of magnetic ones. To create an electric field in the operating gap of the capacitance devices it is enough to have a small amount of the conductive matter. At the same time, to create magnetic field in the operating gap of the induction machines it is necessary to have large amounts of ferromagnetic matter in the form of large magnetic conductor that is used to create opposite magnetic charges at the ends of the gap. This magnetic conductor is the reason for the low energy output of the small energy capacity induction machines.
The parameters of the capacitance electromechanical devices such as driving force, power, reaction time with respect to voltage pulse can be improved by the increase in the field strength in the gaps, as they are proportional to the energy density of the field $\varepsilon\varepsilon_0 E^2/2$, where ε and ε_0 are the dielectric permeabilities of the medium and the vacuum.
Use of the micromachining for the manufacturing of the electrostatic micromotors allows one to reach significantly smaller gaps (on the order of several micrometers), and to get higher values of electric field strength and energy density (Harness& Syms, 2000; Wallrabe et al.,1994; Zappe et al., 1997; Kim & Chun, 2001).
The estimates of specific energy output based on the energy density of electric and magnetic fields can be used to determine the gap width necessary for the electric field energy density to be comparable to or higher than magnetic field energy density (~$4\text{-}5\cdot10^5$ J/m^3 with 1 T induction and very high quality of magnetic material). For 20-60V voltage, the gap is 2 μm. Such a gap that is used in modern electrostatic micromotors results in the higher value of the electric energy stored in the sample, as compared to the classical electrostatic motors, and, consequently, in the better motor efficiency.
With the help of silicon deep etching technology the gaps of about 2 μm can be created, so the specific electric capacitance C_{sp} and specific energy output A_{sp} of the elemental actuator can be as high as 4 pF/mm^2 and 10^{-8} J/mm^2 respectively, and the driving force F can achieve the value of 10^{-6}- 10^{-5} N.
The processibillity in fabrication of electrostatic motors, the simple design and no need to use the magnetic core are the reasons for the dominant use of the electrostatic microactuators in MEMS.

The operation principle of these microactuators is as follows: the moving electrode is pulled in the interelectrode gap with the pulling force equal to $(V^2\partial C/\partial x)/2$ (V is applied voltage, C – total capacitance of the structure). The drawbacks of these microactuators are the small values of the main parameters C_{sp}, A_{sp}, F and the small range of moving element (moving platform, MP) motion – on the order of 5 – 50 μm. To increase the power of the device it is necessary to use many microactuators in parallel and, consequently, use a significant part of the integrated circuit surface. The forces developed by these micromotors are in the range of 1 – 10 μN. This value determines the field of the micromotor applications.

A certain increase of C_{sp}, not more than by one order of magnitude, can be achieved by filling the interelectrode gap by dielectric. The techniques of such energy conversion were proposed in papers (Dyatlov, et.al., 1991; Dyatlov, et.al., 1996; Sato & Shikida, 1992; Akiyama & Fujita, 1995).

On the other hand the thin-film metal-ferroelectric-metal structures have high enough electrical power capacity, which can exceed the corresponding capacity of air gap by thousand times due to high values of ε at higher breakdown strength. To convert even a part of this energy into mechanical one we have use the effect of reversible electrostatic attraction of thin metal films to the surface of ferroelectrics under action of electric field, so called „electrostatic glue".

2. "Electrostatic glue"

The object of study was thin-film structures of a new type synthesized on the surfaces of silicon or sapphire substrates and composed of a ferroelectric film with a high permittivity ε and thickness d and an elastic mobile thin electrode with an air nanogap of thickness d_z between (fig. 1).

The ferroelectric component was a strontium barium—niobate (SBN) film doped with lanthanum ($Ba_{0.5}Sr_{0.5}Nb_2O_6$ + 1% La) and with a permittivity of 3000—5000. The film was synthesized on an ITO (In_2O_3 + 6% SnO_2) electrode surface. The thicknesses of the ITO and SBN films were 0.1—0.5 and 0.3—3 μm, respectively. The preparation technique of the films and their main electrical characteristics were described in (Kostsov, 2005).

During the electrostatic attraction of the petal to the ferroelectric surface the total current consisting of the conductive current and the capacitance current arises in the electric circuit. Our technique allows us to separate these components during in real time.

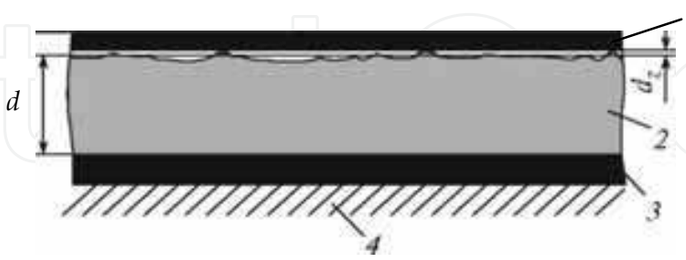

Fig. 1. Schematic diagram illustrating the electrostatic pressing of a metal film (1) to the surface of ferroelectric film (2), deposited on a substrate (4) with a barrier electrode (3)

The voltage pulse applied to the structure was modulated by sine voltage with the frequency equal to 1 MHz and the amplitude equal to 1 – 2% of the total pulse amplitude V. The response to this voltage pulse allows one to measure alternating conduction (in-phase signal) and capacitance (signal shifted by 90°) current, and then one can calculate the transient values of conductivity and capacitance C(t).

Study of C(t) behavior during the electrostatic pressing of the metal and the ferroelectric surfaces performed on the prototype consisting of the large petal (l=10 mm in length and b=1 mm in width) freely lying on the surface of the ferroelectric film (see fig.2) shows that as V grows, the process duration abruptly drops. The C(t) values initially grows, and then comes to the saturated value that is determined by the width of the air gap between the metal and the ferroelectric and the parameters of the BSN film. As V grows further, saturated value of C(t) can fall because the capacitance of ferroelectric layer becomes smaller due to the polarization screening in the ferroelectric. To reduce this effect of polarization charge accumulation it is necessary to apply shorter pulses, use shorter petals and apply bipolar voltage pulses (Baginsky & Kostsov, 2004). With l equal to 1-3 mm pulse duration t_p should be between 50 –500 μs.

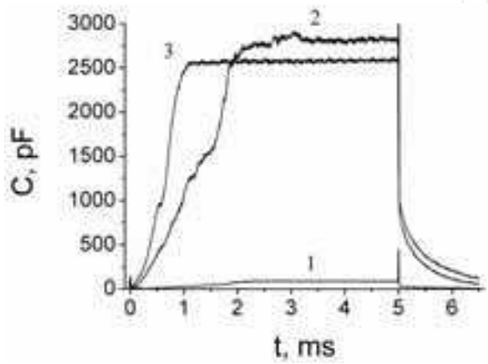

Fig. 2. Time behaviour of the capacitance of the free lying petal – BSN film (d=2.4 μm) – electrode structure when a voltage pulse with duration of t_p=5 ms and amplitude V= **1** – 30, **2** – 40, **3 –** 50 V is applied.

Due to the high ε value, the electric field in the structure under a voltage V is such that the potential drops mainly on the air gap between the mobile electrode and ferroelectric film; i.e., the field is mainly concentrated in the gap, and the specific capacitance of the structure $C_{sp}=k_oC_o$ is several times less than the specific capacitance C_o of the metal-ferroelectric-metal (MFM) structure with the applied electrodes. At sufficiently high values of ε/d the value of C_{sp} approaches to the gap capacitance C_Z, and the experimental studies show that k_o can be about 0.05 – 0.5, see fig. 3a. The field redistribution between the ferroelectric and air gap may occur only at high ε values (specifically, when $\varepsilon/d > 10^8$ m^{-1} (Kostsov, 2008)). Analysis of the field distribution in the air gap for different ε/d values shows that, with a decrease in d_z, the pressing force $F_p=V^2(dC_z/dz)$ for the mobile electrode to the ferroelectric surface nonlinearly increases (fig. 3b). The force significantly increases beginning from a distance of 100 nm or less between the surfaces, and at $\varepsilon/d > 10^9$ m^{-1} one can obtain a pressure of more than 10^4 N/cm^2 in the nanogap. Note that for the linear dielectrics ($\varepsilon/d < 10^7$ m^{-1}) the voltage drop on the nanogap is insignificant. Although the voltage applied to the nanogap is fairly high (up to 100 V or more), it does not cause electric breakdown, because (i) the Paschen law is invalid for such narrow air gaps and (ii) in this structure the ferroelectric film resistance more than 10 MOhm/mm^2 is connected in series with the gap. The breakdown field strength of the ferroelectric film exceeds 100 V/μm, and a low voltage drop directly on the ferroelectric film excludes its breakdown.

The air nanogap width d_z determined by measuring the total capacitance of the structure is falling with an increase in the voltage applied. For a specific sample, the minimum d_z value

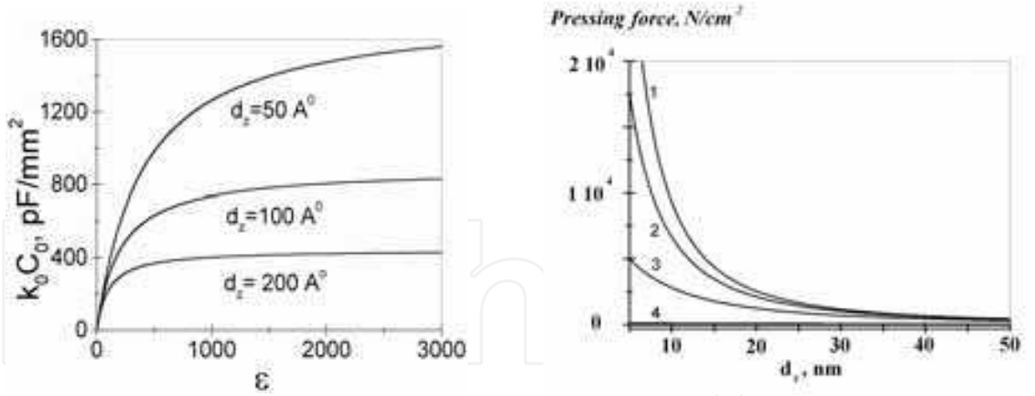

a. b.

Fig. 3. The dependence of specific capacitance on dielectric permittivity value for the system: free metal film-ferroelectric film-electrode for various values of air gap d_Z (**a**): d=2 μm and the pressing force on d_Z value (**b**): ε/d= (1)-10^9, (2)-3.3 10^8, (3)-10^8, (4)-10^7m^{-1}.

is limited by the roughness of the surfaces of both the ferroelectric film and mobile electrode and the specific capacitance C_{sp} of the structure at the instant of pressing the mobile electrode is 10—10^3 pF/mm^2, depending on V.

It was found experimentally that the adhesion force of the electrostatically pressed (using electrostatic "glue") surfaces depends linearly on the electrostatic energy accumulated in the structure and exceeds (3—5) x 10^5 N/J. In particular, a force above 10 N is necessary to separate surfaces 1 cm^2 in area. The pressure in the nanogap may exceed 10^4 N/cm^2; it is determined by the crystal quality of the ferroelectric film and its hardness.

Note that in this case the pressure formed by the electric field in the nanogap greatly (by orders of magnitude or even more) exceeds the pressure obtained in the gaps of large modern devices using stationary magnetic fields close to the maximally possible (to (3—4) x 10^6 A/m). In this case, the decisive factor is the field energy density $\varepsilon\varepsilon_0E^2/2$ or $\mu\mu_0H^2/2$ ($\mu\mu_0$ is the magnetic permeability, H – magnetic field strength), which is measured in J/m^3 and identically equal to pressure in N/m^2. In the case considered here E may reach values up to 10^{10} V m^{-1} and, correspondingly, the energy density can be as high as 4 x 10^8 J/m^3 (pressure up to 10^5 N/cm^2).

We studied the specific features of breaking adhesion of the ferroelectric and metal film surfaces when switching off the voltage. It was established that the time of detachment of the mobile electrode from the ferroelectric surface lies in the nanosecond range (fig. 4a). Such a short detachment time is explained by the existence of two oppositely directed forces on the mobile electrode: the electrostatic force in the gap, formed by the applied voltage V, and a mechanical force, the origin of which is as follows: when the free thin metal film is electrostatically pressed against the ferroelectric surface, a significant part of the energy accumulated in the structure (estimated to be 10^{-3}— 10^{-2} J/m^2 or 1—5% of the electrostatic field energy) is spent on the elastic mechanical deformation of the metal film (beryllium bronze), which is pulled like a membrane on individual microasperities of the ferroelectric surface. The parameters of ferroelectric film surface roughness (the number and height of microasperities) are determined by the preparation conditions and film thickness. After switching off the voltage, the released mechanical energy determines the high detachment rate of the metal film (whose mass is 10^{-9}—10^{-10} g) from the ferroelectric surface for 50—200 ns. It is facilitated by the low space charge in the ferroelectric film and high surface hardness of the ferroelectric (5.5 on the Mohs scale).

To analyze how the surfaces are separated, we investigated the dependence of the structure capacitance relaxation (fig. 4b, curve 2) at a sharp drop of voltage pulse (the trailing edge of which was about 30 ns) from the initial amplitude V a small value V_1 (fig. 4b, curve 1), at which the metal film cannot be retained by electrostatic forces on the ferroelectric surface. We took into account that the conduction currents through the structure are negligible in comparison with the capacitance discharge current.

The effect considered here, see also (Baginsky & Kostsov, 2010), makes it possible to generate and remove strong forces of reversible adhesion between two surfaces at high clock frequencies, and it is the basic for the creation new type of micromotors and other MEMS devices.

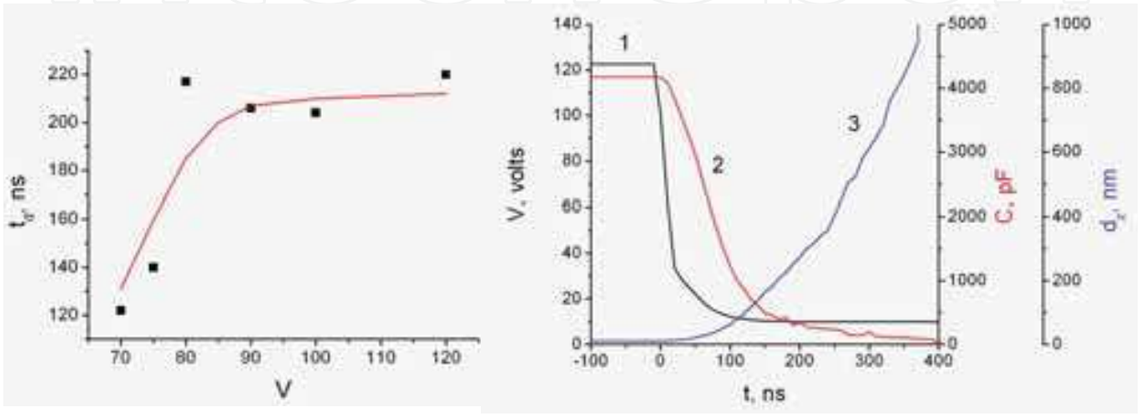

a. b.

Fig. 4. Separation of the surfaces of a free metal film and ferroelectric at switching off of the voltage pulse (for the structure mobile metal film (beryllium bronze, 1.3 μm)- SBN film (2.4 μm)- electrode): (a) the dependence of the surface separation time on the voltage pulse amplitude and (b) separation of the metal film and ferroelectric film surfaces at switching off of voltage: (1) V(t), (2) C(t), and (3) $d_z(t)$.

3. Effect of rolling and the principle of micromotor operation based on this effect

The effect of rolling is a certain kind of electrostatic attraction of thin metal film, named below as a petal, at which the attraction is expanding gradually part by part from one end of the film to another.

The petal moving under the effect of the electrostatic force along the ferroelectric surface can transfer the motion to the external object (moving plate) upon bending, and thus carry out the electromechanic energy conversion. The movement velocity of the petal part that is rolled on the ferroelectric and the accumulated energy (transferred into mechanic energy) are defined by the voltage amplitude, ferroelectric film thickness and ε value. The evaluations show that the pressure in the interelectrode gap at the instant of the contact of the two surfaces (starting from the distance 10 nm) is equal to 10^4 – 1.5 10^4 N/cm^2 and the strain force of the metallic film can be as high as 100 N/mm^2 and more.

The schematic of the use of the electrostatic rolling for the conversion of the electric energy accumulated in the ferroelectric into the kinetic energy of the substrate motion is shown on fig.5.

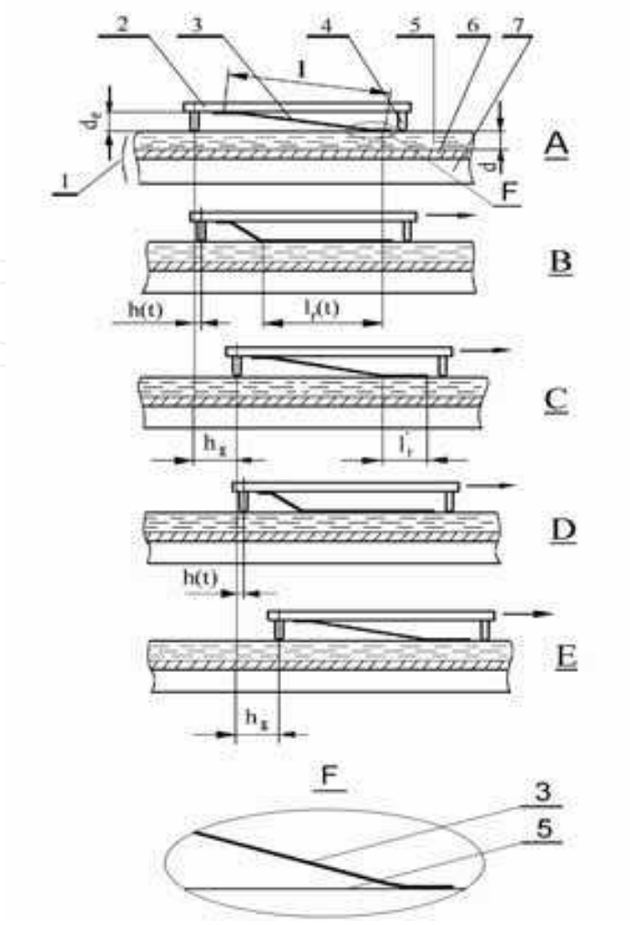

Fig. 5. A scheme illustrating for the motion effects for the petal micromotor. **A** – initial state and position, t = 0; **B** – the state and position at the end of the first voltage pulse, t = t_p; **C** – the state and position, corresponding to the t = T=1/f; **D** – the state and position at the end of the second pulse; **E** – the state and position, corresponding to the time t = 2T. The initial form of the petal at the contact with the surface of stator is shown in view **F**.

The stationary plate (stator) 1 consists of the silicon substrate 7, with the electrode 6 and ferroelectric film 5 applied to its surface. Petals 3 of length l are attached to the moving plate (slider) 2 that is located at the distance d_e from the stator. Slider moves with respect to stator along the guides 4. In the initial state A the ends of the petals are mechanically pressed to the stator surface, which facilitates the subsequent electrostatic adhesion (see view F). The motion consists of the several stages.

When the voltage pulse is applied between the petal 3 in its initial state A and the electrode 6, the electrostatic adhesion of the petal's end 3 and the ferroelectric film 5 takes place. Then the motion of the plate 2 starts because larger part of the petals' surface is rolled on the ferroelectric surface, and the petals are bent and mechanically stretched. Thus, the electromechanic energy conversion takes place. The rolling length $l_r(t)$ grows with the voltage pulse action time t. Therefore, the shift of the slider h(t) grows too. h(t) value and the speed of the petal's part that is being rolled on the ferroelectric depend on the mass m of the slider, the duration of the voltage pulse t_p, it's amplitude V and the friction coefficient k.

Force F that causes the motion of the slider is applied along the free (not pressed to the stator surface) part of the petal, fig.6. The tangential component of this force F_1 is the driving force, and the normal component F_2 increases the pressure between the slider and the guides. For the efficient energy conversion d_e/l ratio should be sufficiently small, less than 0.1 –0.2.

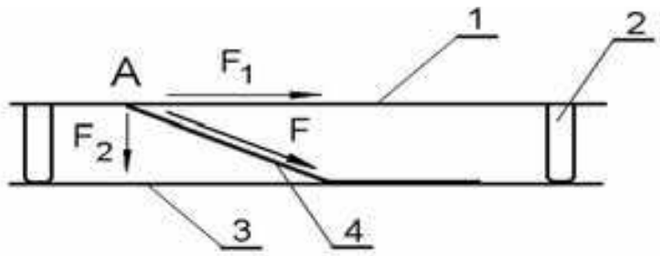

Fig. 6. A scheme illustrating for the pulling force application. 1 – moving plate, 2 – guides, 3 – stator, 4 – petal. A is the point of the force application.

After the end of the voltage pulse the elastic forces bring the petal either to the initial state A (with the single voltage pulse) or to the intermediate state C typical for the continuous movement of the slider (when a series of pulses with the frequency f is applied to the sample). During this time, inertia causes slider to travel the distance h_{Σ}. The time necessary to separate the petal from the ferroelectric surface and to bring petal to the initial shape defines the space between the voltage pulses and, consequently, the maximum pulse frequency and the motor power.
When the second pulse is applied to the sample, the plate makes one more step and comes to the state D. After the end of the second pulse, the slider comes to the state E because of inertia. With the third and further pulses the moving pattern is similar – from position B to position C, etc.

4. Numeric modeling of the electrostatic rolling

To analyze the operation of the linear micromotors in the step regime the mathematical model of the electrostatic rolling was developed based on the energy balance (Dyatlov& Kostsov, 1998, 1999). The redistribution of the electric energy accumulated in the structure during the electrostatic rolling between the kinetic energy of the slider, the work of the load force of the motor (friction) and the petal deformation energy A_d is considered. The parameters of the model are the dimensions of the petal, the Young modulus of the petal material, the motor characteristics (d_e, m, k values), and the voltage source characteristics (t_p, V).
The specific energy of the electrostatic rolling a_r is defined as $a_r = k_o C_o V^2/2$, where $k_o C_o = C_{sp}$.
The work of the electrostatic rolling can be expressed as $A_r = a_r S_r$, where $S_r = b\, l_r(t)$ is the rolling area of the petal during the voltage pulse action. A_r is distributed between the kinetic motion energy, friction force work (effective load) and the deformation energy of the metallic film A_d:

$$A_r = \frac{m}{2}\left(\frac{dh}{dt}\right)^2 + \int_0^h F(x)dx + A_d \,, \tag{1}$$

where x axis coincides with the motion direction. In the first approximation, the shape of the bent part of the petal is described by the cubic parabola with the smooth contact between the petal and the ferroelectric surfaces, see fig. 7.

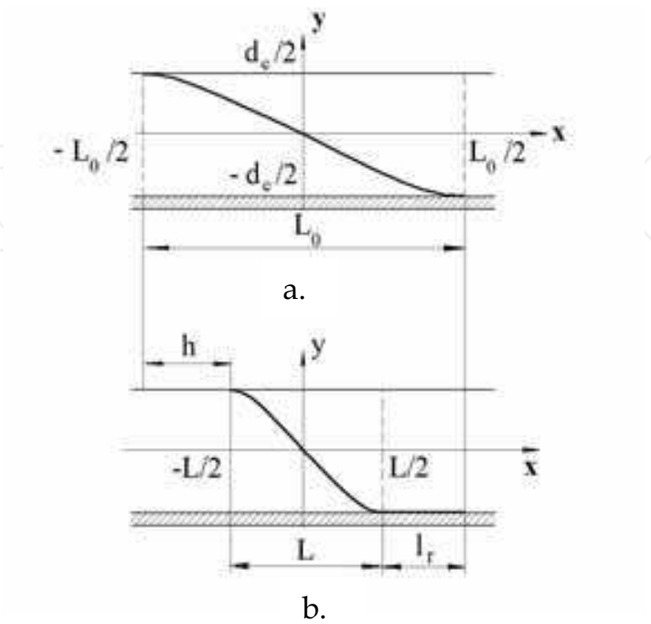

Fig. 7. A scheme for the designations of mathematical model. (**a)** – initial state of the petal, (**b)** – some intermediate state in the process of rolling.

Fig.8 shows the curves characterizing the typical behavior of the single petal motor during the single voltage pulse for 4 different loads. Fig. 8a shows the load force F, fig.8b – the rolling length l_r, fig.8c shows the rolling speed, and fig.8d shows the step h. Other parameters are: L_0 = 4 mm (see fig.7), b = 1 mm, d_e =0.2 mm, k = 0.2, a_r = 0.3 J/m^2, which corresponds to C_{sp} equal to1000 pF/mm^2 at V = 24.5 V.

This figure shows that right after the start of the voltage pulse the motor develops the highest motive force, up to 1-10 N per 1 mm^2 of the rolling area. This force drops later, because as the slider moves the petal tension decreases. The higher the load the more efficiently is the electrostatic rolling energy used. Thus, for the efficient electrostatic rolling energy utilization, t_p value has to be optimally adjusted for the load.

After the end of the voltage pulse the slider continues to move because of inertia, and at a certain time t_{st} determined by the friction coefficient and the slider speed it comes to rest.

The acceleration of the slider depends on its mass and it can be as high as 10000 g when the slider mass is equal to the mass of the petal.

The conversion of the electrostatic rolling energy into different forms of energy for the two different loads (0.1 and 10 grams, respectively) is shown on fig. 9 (a and b). Here the curve 1 describes the increase in the total energy use from the external source during the electrostatic rolling. Curve 2 shows the kinetic energy $mv^2/2$ (v is the slider speed), curve 3 – the energy spent to overcome friction, curve 4 – the work necessary to bend the petals (the work against the elasticity forces). The energy redistribution is time-dependent, the nature of this redistribution is defined by the motor parameters. The parameters can be optimized in such a way that 80-90% of the electric energy will be converted into mechanic energy of the slider

motion. The energy spent on the petal bending will be small, and the electrostatic forces would mainly act to stretch the petals. The estimates show that the stretch forces are much less than the elastic limit of the material. The bending deformation is potentially more serious, but, if the moving plate is sufficiently loaded, it is small, too. Thus, despite the small thickness of the petals, the motor can develop high forces without irreversible petals deformation.

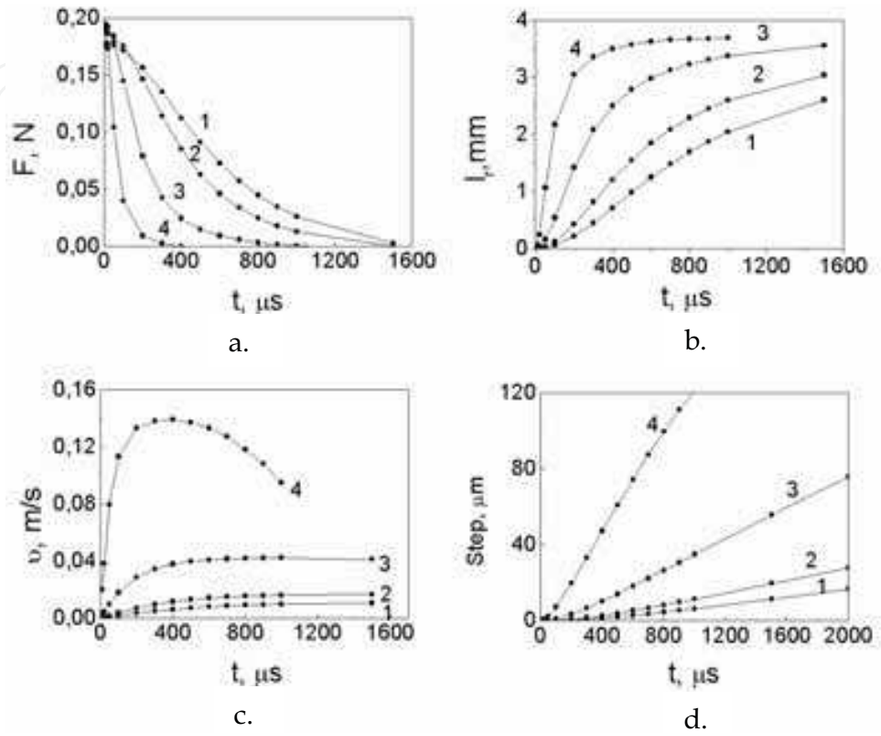

Fig. 8. The theoretical dependencies on the single voltage pulse duration of the following characteristics: (**a**) - traction force, (**b**) - rolling length, (**c**) and (**d**)- velocity and step of micromotor, respectively. m=50, 10, 1 and 0.1 g for curves 1, 2, 3 and 4, respectively.

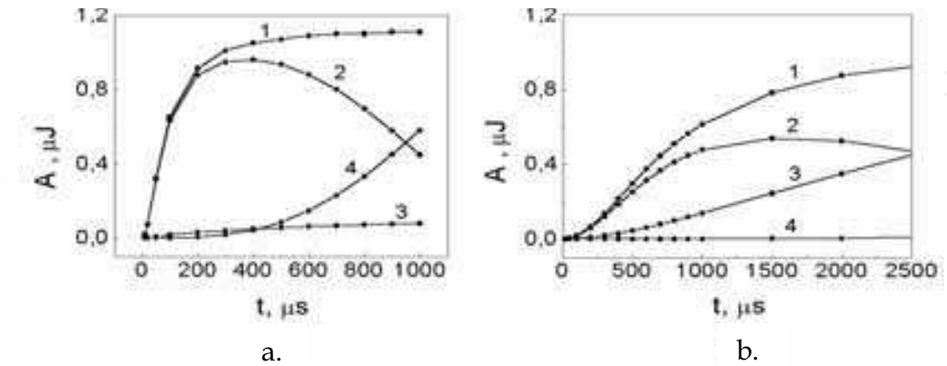

Fig. 9. Energies redistribution in the process of rolling for two different loads: m = 0.1 and 10 grams for figs. **a** and **b**, respectively. Here the curve 1 describes the increase in the total energy use from the external source during the electrostatic rolling. Curve 2 shows the kinetic energy $mv^2/2$, curve 3 – the energy spent to overcome friction, curve 4 – the work necessary to bend the petals (the work against the elasticity forces).

5. Studied structures

Each of the studied samples consisted of the two substrates with the 100-200 μm gaps. The lower (silicon) substrate was stationary one. Metallized ITO and $Ba_{0.5}Sr_{0.5}Nb_2O_6$ ferroelectric films were subsequently deposited by the RF-sputtering on the stationary substrate. The ferroelectric used was barium-strontium niobate ($Ba_{0.5}Sr_{0.5}Nb_2O_6$, BSN) with the dielectric permittivity of about 2000-4000. The ITO and BSN films thickness was 0.5 - 1 and 1 - 3 μm respectively. The BSN films are textured with the crystallographic axis C normal to the substrate surface. The crystallites dimensions were 0.3 – 1 μm. The techniques used to obtain the films and their electrophysical properties are described in (Kostsov, 1995; Kostsov & Malinovsky, 1989; Antsigin et al., 1985).
The matrix of the beryllium bronze (2% beryllium) petals with the length l (1 - 4 mm), width b (300-500 μm) and thickness d_p (1.5-2.5 μm) was formed on the moving substrate, see fig.10. This substrate was the optically polished glass plate 0.5 mm in thickness. All the petals had the common electric contact wire (sputtered during the fabrication of the bronze layer) to apply the voltage. The petals became free by etching of the aluminium sacrificial layer from under the petals. To provide for the reciprocal motion, two groups of the petals were created.

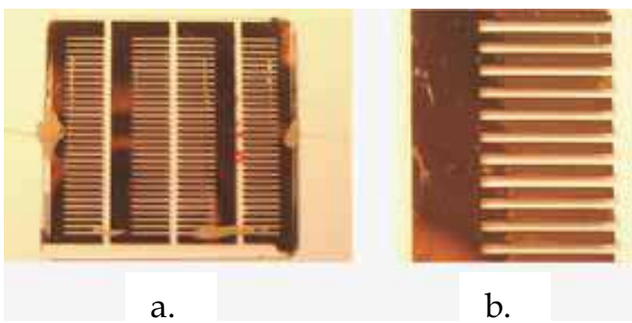

Fig. 10. An example of matrix of the petals design (**a**) and the fragment of the matrix (**b**). Petal size is 0.4*3.5 mm.

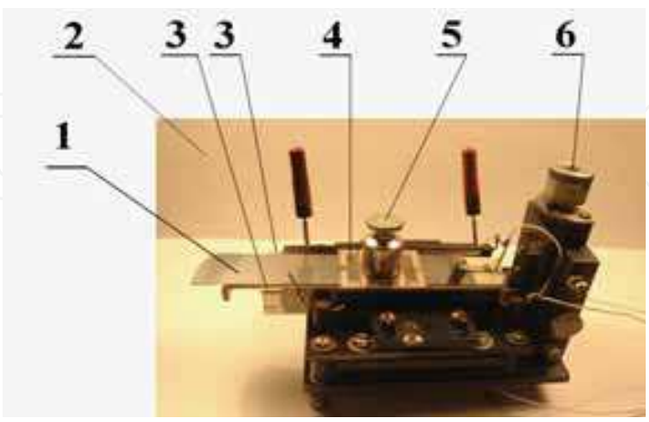

Fig. 11. The experimental set for testing the motor operation. **1** – the bottom substrate (stator), **2** – wires for the contact with the moving substrate, **3** – guides, **4** – moving substrate (slider), **5** – load, **6** – micropositioner for the precise installation of the gap between stator and slider.

The stationary substrate (lower one on the fig.5) and the moving substrate were assembled to form the motor. Two guides were placed between the substrates. For the experiments the probe station was used that allowed one to replace both substrates and adjust the gap between the substrates with good accuracy, see fig. 11.

6. Experimental techniques

To measure the microscopic shift of the slider on the microsecond time scale, the optic technique was developed shown on fig.12. The contrast black-and-white image 2 was attached to slider surface. This image was lit by light beam 6 from laser 7. The image was overlaid with the gap situated in the optical focus of the microscope (lenses 4 and 5) with K-fold zoom. Through the lens 5 the image went to photomultiplier 8. It is easy to show that the electric signal from the photomultiplier will be proportional to the image 2 shift, and the optical resolution of the system will be increased by a factor of K. With K=50 the resolution of about 30 nm was achieved, fig.13.

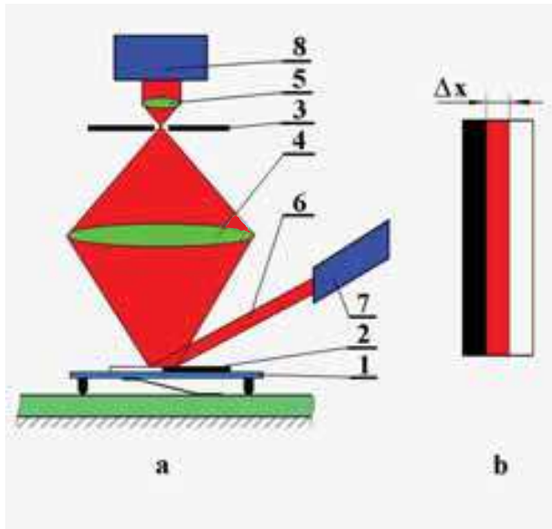

Fig. 12. A method for the optical control of the sample positions. (**a**) is the optical scheme and (**b**) is the image of black and white contrast (**2**), restricted by optical gap (**3**) after the microscop ocular (**5**), Δx is a shadow. **1** – moving plate, **2** – black and white image, **3** – optical gap, **4** – objective lens, **5** – ocular lens, **6** – laser beam, **7** – laser, **8** – photomultiplier.

To separate the components of the total current (capacitance charging current and conduction current) during the electrostatic rolling the integrating technique suggested in (Yun, 1973) was used (see fig.13). The rectangular voltage pulse from the generator 4 was applied to the sample 1 with the time-dependent capacitance C(t) and resistance R(t). The time integral of the current passing through the sample was determined by measuring the potential φ(t) on the measuring capacitor C_m>>C(t), connected in series with the sample 1. Then the signal was amplified (2) and supplied to the analyzer 3 (e.g., oscilloscope). Here

$$\phi(t) = Q(t) / C_m \text{ , where } Q(t) = \int_0^t I(t)dt \text{ -} \tag{12}$$

is the total charge, I(t) – total current, $t<t_p$, where t_p is the voltage pulse duration.

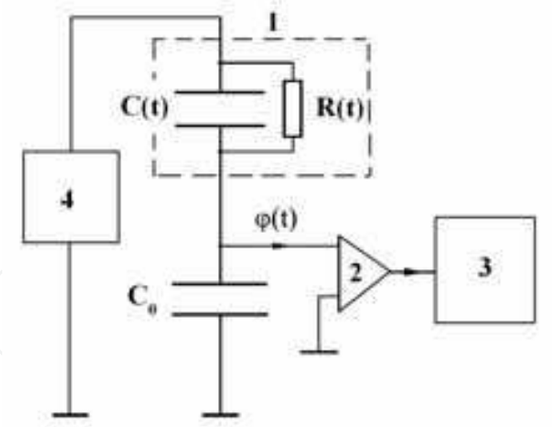

Fig. 13. A schematic representation for the method of capacitance and conductance current separation. **1** – a sample, consisted (schematically) of time-dependent values : C(t) and R(t). $\mathbf{C_0}$ is the measuring capacitance, φ(t) is the measured potential; **2** – amplifier; **3** – oscilloscope; **4** – voltage pulse generator.

Since after the end of the voltage pulse the time Δt necessary to discharge the capacitor C(t) is short and does not depend on the mechanism of the discharge, we have

$$\phi_1(t_p) = \phi(t_p + \Delta t) = \frac{\int_0^{t_p} I_c(t)dt}{C_m} = Q_c(t_p) / C_m \,, \tag{13}$$

where I_c and Q_c are the conductivity current and it's integral, respectively. Then

$$Q_{cap}(t_p) = \left(\varphi(t_p) - \varphi_1(t_p)\right) C_m \quad \text{and} \quad C(t) = Q_{cap}(t) / V, \tag{14}$$

where Q_{cap} is the charge accumulated at the capacitance C(t),V is amplitude of voltage pulse. Thus, by measuring $Q(t_p)$ and $Q_c(t_p)$, it is easy to determine C(t), $I_c(t)$, $I_{cap}(t)$, where $I_{cap}(t)$ is the capacitance charging current. Thus, we separate the conductivity current and capacitance charging current.

The macromotion of the slider was measured using the optical microscope, and the time during which this motion occurred was measured by the number of the voltage pulses and their frequency.

7. Experimental studies of thin-film petal micromotors

The studies conducted with the samples described above, see (Baginsky & Kostsov, 2007), showed that mechanical and electric characteristics qualitatively correspond to the theoretical estimates for the relatively slightly bent petals. In this case the energy conversion efficiency is 60-70% with the rolling time of 1.5-1.7 ms. But relatively low operating frequency (100 Hz and less, see fig.14, curve 3) causes the micromotor to operate with low power. The resonance frequency at which the slider speed reaches maximum corresponds to the resonance frequency f_r of the oscillations of a cantilever with the length l (where l is the petal length):

$$f_r = 0.162 d_p / l^2 (E_Y / \rho)^{1/2}, \quad (17)$$

where d_p is the thickness of the petal, E_Y is the Young modulus, ρ is specific weight. With the petal thickness of about 1.5-2 μm and the Young modulus for berillium bronze $E_Y=10^{11}$ N/m², f_r = 40-60 Hz.

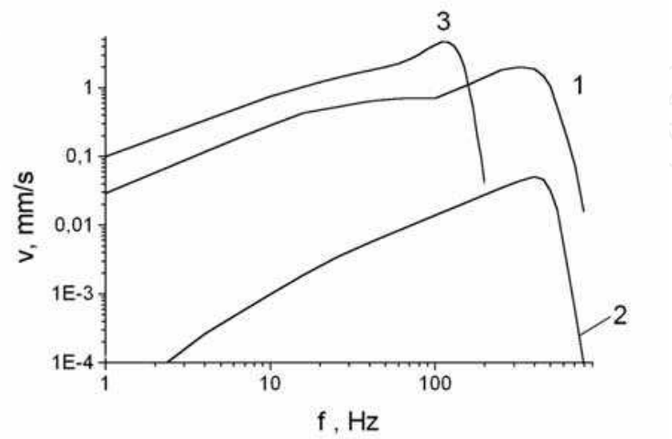

Fig. 14. The frequency dependence of the sample velocity for the cases of bent petals in cross- sectional view (1, 2) and straight petals (3). V=50 V: (1), (3) and V=30 V: (2)

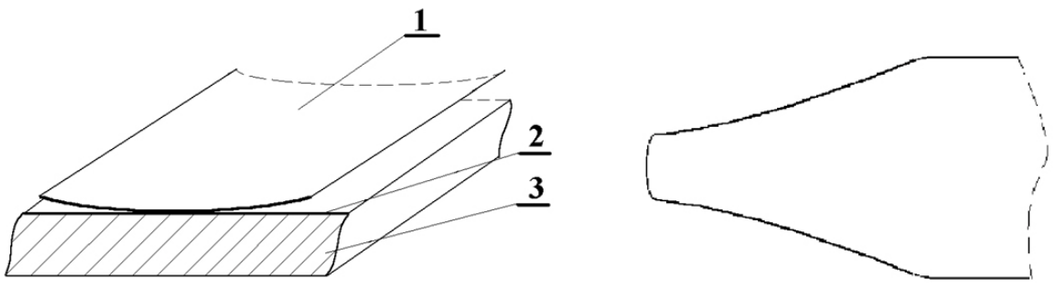

a. b.

Fig. 15. A view of the bent petal at the position of it's contact with the lower substrate (**a**) and a scheme for the contact surface between the petal and lower substrate (**b**). **1** - petal, **2** – the surface of lower substrate (**3**).

Thus, the most important problem is to increase the clock frequency of the micromotor operation. One of the possible solutions is to use the 3D petals structure, when the radius of curvature of the petal cross-section is comparable to petal width b. The cross-section of this petal (1) at the point of contact with the lower substrate (2) is shown on fig.15a. In this cross-section, the petal acts as a spring with the curvature radius r>b. The lateral cross-section of the petal is straight, with the exception of the contact area with the stator, where the petal is bent (see fig. 5F). During the electrostatic rolling of the petal, this spring is attracted to the ferroelectric surface, and its resonance frequency is determined by its width b, and, if it's length l>>b, is almost independent on length and the applied voltage. It was checked experimentally – the resonance frequency is close to the f_r value obtained when l in equation (17) is replaced with b, see fig. 14, curves 1, 2, in contrast to the straight petals, when the f_r value is determined by their length (curve 3).

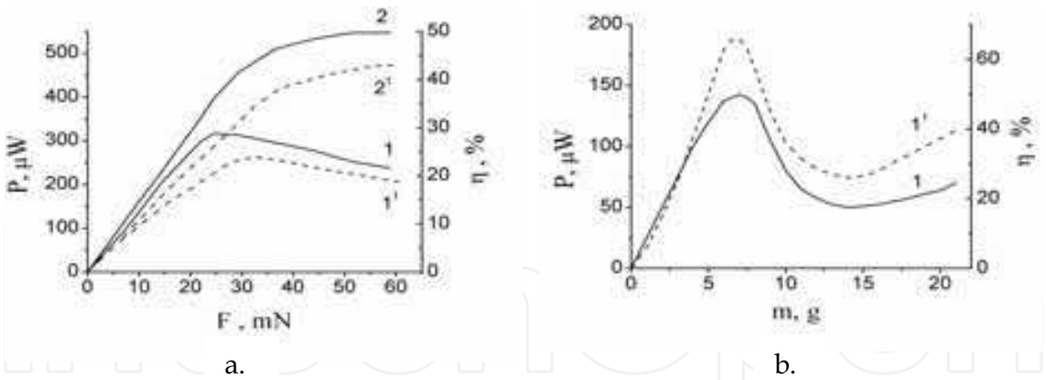

a. b.

Fig. 16. Power (solid lines) and energy conversion efficiency (dashed lines) as a function of load for the U-shaped (**a**) and flat (**b**) petals with the mass loading (curves (**1**)) and the friction loading (curves (**2**)). The number of petals N=40, f= 1 kHz (**a**), f=100 Hz (**b**).

Moreover the experiments revealed an unusually fast separation of the metallic films (petals) from the ferroelectric surface after the end of the voltage pulse action, discussed above in Sect. 2.

Thus, two factors are identified that can increase the operating frequency of the micromotor. The first one is fast separation of the surfaces; the second one is connected with the 3D petal structure.

The load parameters of the micromotor with 3D petals for the operating frequencies that are close to the optimal ones are shown on figs. 16a and 17. With the mass load, one or more clearly identifiable power peaks were observed, that can be explained by inertia properties (fig.16a, curve 1 and fig.17a, b). The comparison of the load properties of the micromotor for the mass and friction loading, see fig. 16a, have shown that the application of the friction loading should increase power and efficiency (η) of the electromechanical energy conversion. With the friction load, the power was independent on the load value at high enough loads (fig.16a, curve 2). Under these conditions with sufficiently large load, the motor abruptly stopped with further load increase. The power peak (mass load) or plateau (friction load) correspond to switch from the inertial mode to the step mode. In the step mode, the motor comes to stop between the voltage pulses.

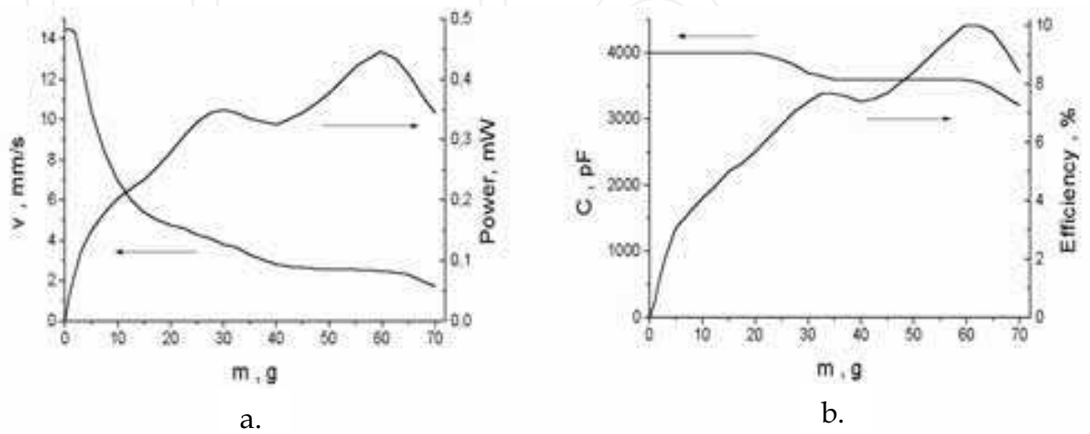

a. b.

Fig. 17. The multiple peak structure of load characteristics at mass loading.

The relatively low efficiency in the case of U-shaped petal is explained by the fact that in the resonance determined by the petal width only a small part of the petal length comparable to its width participates in the rolling in the stationary periodic mode, and the rest of the petal length spreads along the ferroelectric surface and is periodically attracted to and repelled from it without participating in energy conversion process. So the petal takes the shape of "bulldozer knife".

Higher efficiency can be achieved with the flat petals, but the voltage pulse repetition frequency consistent with the resonance frequency becomes lower, relative pulse duration decreases, and specific power is reduced despite increase in the specific energy, see fig. 16b.

Thus to achieve maximum mechanic power and electromechanical energy conversion efficiency the rolling time must be consistent with pulse repetition frequency. This can be achieved by selection of optimal size and shape of the petals. It can be concluded from the reasoning above that to achieve maximum efficiency the petals must be flat, and to achieve maximum power their length should be decreased. In particular, for operating frequencies on the order of 1 kHz their length should be about 1 mm.

The examples of the slider acceleration as a series of voltage pulses is applied are shown on fig.18 for inertial (a) and step mode (b, c). Here, the pulse length is 0.4 ms, and the pulse repetition rate is 1 ms. In both cases, the slider speed would come to plateau at the second pulse at high energy output (with high V). As V decreases, more pulses are necessary for the complete acceleration, see fig.18a.

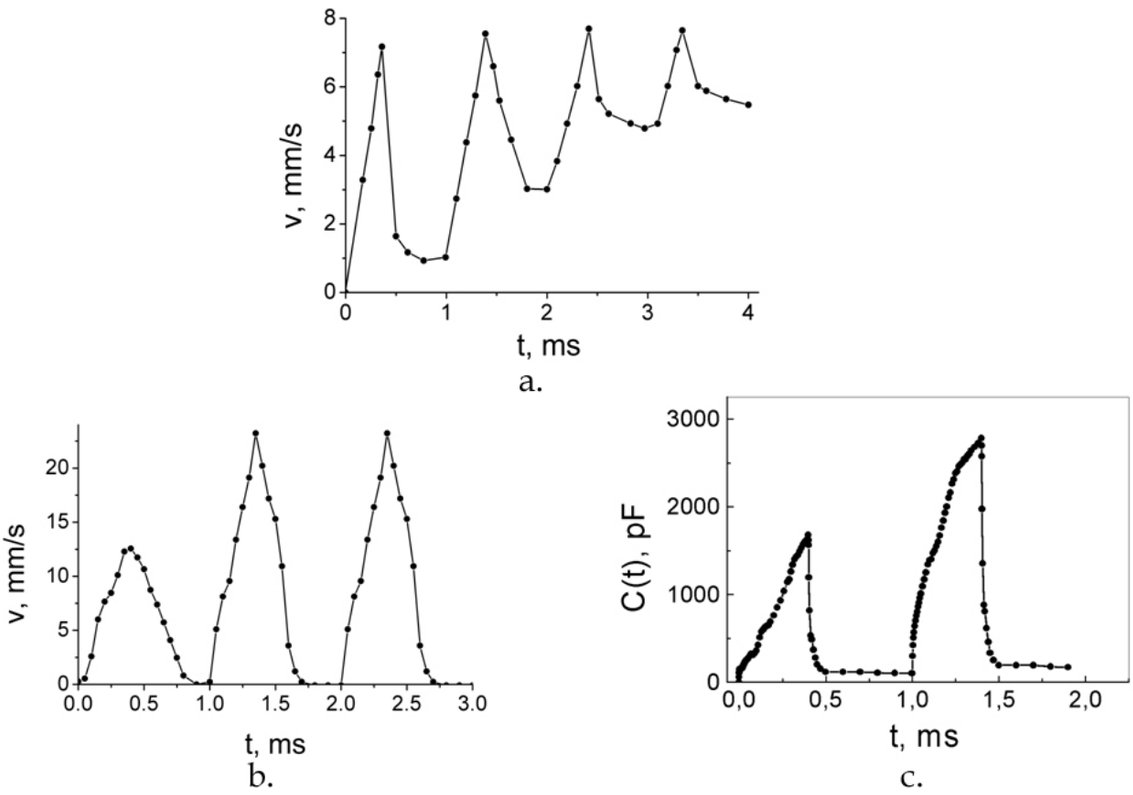

Fig. 18. Slider acceleration in the inertial mode (a) and in the step motion (b). N = 40. (**a**): M=0.5g, V=40 V, (**b**): M=5g, V=50 V and (**c**) time variation of the sample capacitance at step mode regime corresponding to Fig.18b (first two steps).

Finally, let's discuss the method of increasing the energy conversion efficiency and power output. Fig. 18b shows the acceleration of the slider in the step mode. The acceleration time depends on the amplitude V. The fact that both power and energy conversion efficiency are higher starting from the second, third, etc. pulse (see fig.18 b, c) means that petals tension increases in the equilibrium step mode. The increase in petal tension can also explain the power increase as the load increases. Thus, after the end of the acceleration stage the efficiency increases and can reach rather high values.

In the equilibrium mode significant fraction of the petals capacitance is not used for the energy conversion, as part of each petal's surface remains parallel to the stator surface because it does not have time to come to the initial state, thus assuming the shape shown on fig. 5c. This shape can be visually observed with the continuous slider motion. On the curves showing C(t) as a function of load this petal shape manifests itself through the large part of the capacitance that is independent on the load value (see fig.17b). Thus, efficiency and power dependences on the load are similar (see fig.16, dotted line corresponds to curve 1-P(F) for the mass load) and fig.17. Significantly more rapid C(t) growth starting from the second, third etc. voltage pulses (see fig.18c) can also be explained by the electrostatic attraction of the part (about 50% according to the estimates) of the petal that did not significantly separate from the ferroelectric surface in the pause between the pulses moving almost parallel to this surface. So when the next voltage pulse is coming this part of the petal is attracting to the ferroelectric surface much more rapidly compared to the first pulse.

The accumulation of the space charge in the ferroelectric leads to the decrease in the efficiency of the energy conversion. This accumulation is connected with both polarization and the injection of the charge carriers under the action of the voltage pulse. After the end of the voltage pulse the electric field still exists on the ferroelectric surface. It attracts the petal and does not allow the petal to assume the initial state. Thus, it interferes with the slider motion in the pause between the voltage pulses. Besides, when the next voltage pulse comes to the ferroelectric surface, the residual potential on the ferroelectric surface when added to the applied voltage decreases the electric field in the metallic film – ferroelectric surface gap. Both these factors lead to deceleration of the slider, and the decrease in the motor power. One of the ways to eliminate the space charge accumulated during the action of the main voltage pulses is the application of the additional pulses (AP) of the opposite polarity in the pauses between the main pulses. Similar processes to alter the potential of the surface at the semiconductor-dielectric boundary with AP are used in the MNOS memory elements (Yun, 1974).

The configuration of the voltage pulses is shown on fig.19d, and the slider speed as function of the additional pulse amplitude V_1 is shown on fig.19a. As the shift between AP and the main pulse grows, its effect on the slider speed increase disappears, see fig.19b. The data shown on fig.19 can be explained by the two phenomena: the compensation of the space charge and the deceleration of the slider due to the application of voltage pulse V_1, even if for a short time. When AP is applied right after the main pulse, the deceleration plays positive role, leading to the separation of some part of the petals from BSN surface even with applied AP. The latter effect manifests itself through the decrease in the capacitance C some time t after the start of AP (see fig.19c). The following AP parameters were chosen experimentally: amplitude V_1= -17 V, duration t_1 = 50 μs. With these AP parameters the speed of the slider and the micromotor power are by a factor of 1.5- 2 higher as compared with the mode when AP is not used.

The main reason for the decrease in the energy conversion efficiency as the petal assumes the form shown on fig.5C, which excludes part of the petal from the energy conversion process is the mismatch between the frequency corresponding to the motor's maximum power and the natural frequency of the petal's vibrations. For example, for the petals

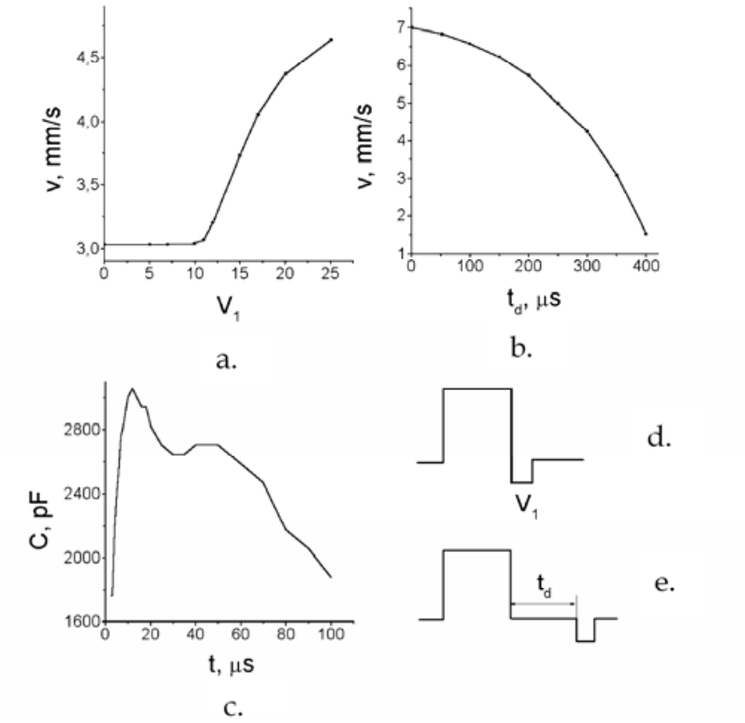

Fig. 19. The characteristics of the motor behavior under conditions, when additional voltage pulse (AP) is applied. **a** – the dependence of slider velocity on the amplitude of AP – V_1 (configuration **d**), **b** - the dependence of slider velocity on the delay between main and additional pulses – τ_d (configuration **e**), **c** – the dependence of the structure capacitance on the AP duration.

shape shown on fig. 15a with the operation frequency of 1 kHz, the on-line time ratio of the pulses was 0.5, yet the efficiency was less than 20-25%, because the resonance of that frequency corresponded to petal's width. In case of flat petals, the efficiency was 70-80%, but the operating frequency decreased to 100-40 Hz, which resulted in the on-line time ratio increase by a factor of 10-20. Thus, despite the increase in the mechanical energy generated during one conversion cycle by a factor of 3-4, the power was fallen down by a factor of 3-5

The second reason for the incomplete conversion of the rolling capacitance energy into the mechanical energy is the incomplete rolling of the petal's surface, that is, the formation of the so called rolling needle shown on fig.15b. The formation of this needle can be attributed to the difference in the speed v_l of the longitudinal (along the petal's length) rolling and speed v_b of the lateral rolling, because initially the petal has the 3D structure shown on fig.15a. This results in the motive force decrease, because in this case only the part of the petal's width that is on the front end of the rolling contributes to the driving force (see fig.15b). It can be noted that this phenomenon can explain the possibility of the significant efficiency increase with the practically unchanged power by increase in the petal's stiffness achieved by small increase in the thickness. In this case the efficiency increase with the rolling capacitance decrease can be attributed to the decrease in the unused capacitance. This happens because relatively smaller part of the lateral surface of the petal is rolled because of the increase in the lateral stiffness. The above mechanism can explain steep

(faster than quadratic) growth of P as a function of V at the low voltages. At high voltages, P is quadratic function of V, because the growth in voltage increases the lateral rolling speed and leads to the rolling needle disappearance.
The decrease in the petal length accompanied by appropriate (roughly proportional) decrease in the gap thickness d_e allows one to achieve the resonance motion of the slider with respect to the petal length, and thus achieve high efficiency accompanied by the specific power increase. To increase power by an order of magnitude it is necessary to use 0.5 mm and shorter petals.

8. The peculiarities of ferroelectric ceramic application in petal micromotors

To create micromotor prototype thin ceramic plates were used made of PZT material with the composition Pb0 - 66%, ZrO_2 - 21%, TiO_2 - 11% and dielectric constant of $\varepsilon_F \sim 3900$. Also, we used plates made of antiferroelectric ceramics with the composition close to PZT and dielectric constant of 10000. The surfaces of the ceramic plates used for the electrostatic rolling were polished up to the optical smoothness (roughness of about 10^{-8} m). The metallic electrode (silver film with 1 μm thickness) was applied to another ceramic surface by vacuum deposition followed by sintering.
One of the peculiarities arising from the use of the ferroelectric ceramics in the described construction, as opposed to the use of barium-strontium niobate films (Dyatlov et al., 2000; Baginsky & Kostsov, 2003) is higher value of the switched polarization part and longer time before polarization disappearance.
To significantly decrease the effect of the polarization switch in the step mode, it is necessary to apply the pulse of the opposite polarity with length and amplitude sufficient to bring the polarization direction into its initial state before the application of the slider moving pulse. But even this scheme of voltage pulse application does not completely solve the problem of polarization screening charge, since between the pulses there is an electric field near the ferroelectric surface that causes the slider to stop and decreases the motor power.
The investigations of micromotors made on the basis of PZT ceramics revealed only a small values of mechanical energy and specific power because of high values of polarization damping the motion.
The effect of the polarization processes can be significantly decreased by using antiferroelectric materials with high ε, that are shown to have quite small or no residual polarization (Burfoot & Taylor, 1979).
The ceramics was 100 μm thick, with the specific capacitance of about 900 pF/mm². The specific capacitance during the electrostatic rolling was only 20 – 40 % smaller than that of the ferroelectric films despite higher thickness. Since the use of AFE ceramics allows one to apply significantly stronger voltage pulses than would be possible for the ferroelectric films without compromising the operation reliability, it is obvious that the energy capacitance and motor power can also be significantly increased.
Fig. 20 shows the frequency (a) and load (b) properties of the micromotors based on the AFE ceramics for the constant number (n=40) and size (3.5*0.5mm) of petals and their dependence on the voltage pulse duration (c). To eliminate the effect of the space charge that is created by the leakage current caused by the voltage pulse, after the end of the main pulse (MP) the additional pulse (AP) was applied with the amplitude equal to that of the MP, but of the opposite polarity and with smaller duration (100 μs). This relationship between MP and AP parameters was found experimentally to maximize the power of the micromotor with the given load.

The analysis of the frequency properties of the motor power (fig. 20a) showed the resonance at clock frequency of about 1 kHz. The resonance position was virtually independent on voltage pulse amplitude and motor power and load. It shows that the peak can be mainly attributed to the mechanical resonance based on the petal width.
For the fixed load and voltage pulse amplitude the micromotor power can be maximized by adjusting the pulse duration and the time between the pulses. For example, fig.20c shows the typical curve of micromotor power as a function of pulse duration, with the optimal pulse duration of 450 μs. The complex shape of this curve with two maximums is explained by manifestation of two effects. The first peak appears due to the mechanical resonance of the petal at frequency of about 1 kHz (Baginsky & Kostsov, 2003). As the pulse duration t_p grows at the conditions of fixed gap between the pulses Δt the additional part of the petal's length is involved in the process. It gives rise to the additional grows of power despite of the frequency $f = 1/T$ (where $T = t_p + \Delta t$) decrease, so the second peak is forming.
Load curves, fig. 20b show the power peak at 40 g load (the friction coefficient k is 0.3). The maximal power was 1.5 mW, which is 2-3 times greater than for the similar motor based on the ferroelectric films.

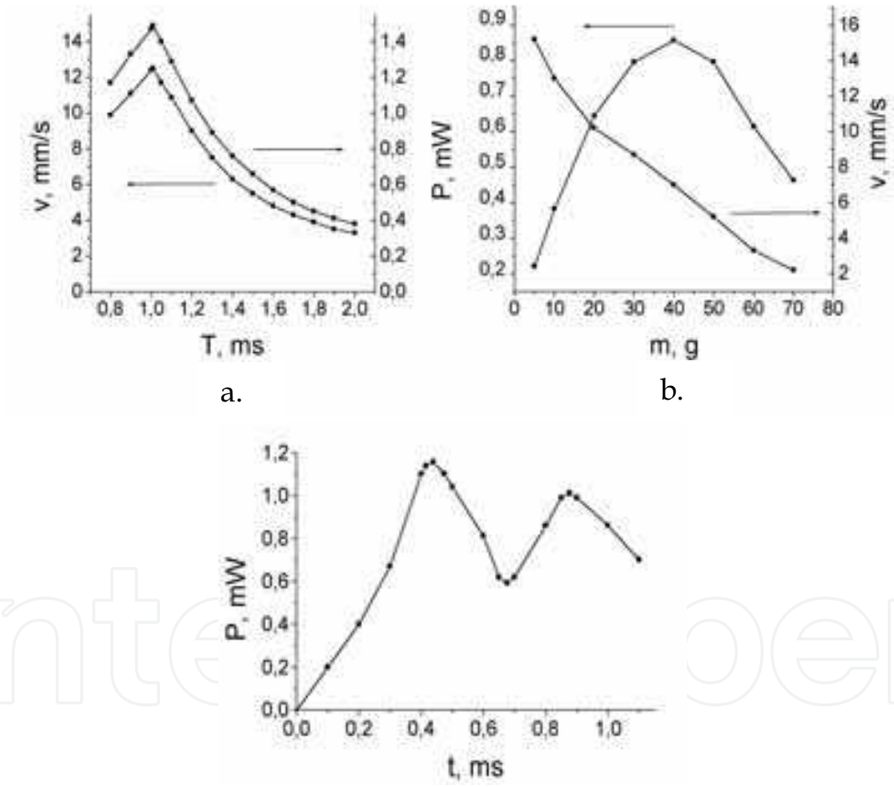

Fig. 20. Power and speed of the antiferroelectric ceramics motor, (**a**) – as a function of voltage pulse period (m = 40 g, t_p = 0.45 ms), (**b**) – of the load mass (T = 1 ms, t_p = 0.4 ms) and (**c**) - of the voltage pulse duration. m = 40 g, V = 85 V, t_1 = 0.1 ms.

Table 1 compares the maximal absolute and specific power, P and P_1, with the same mass load, friction coefficient (k=0.3) and number of petals (n=40) for motors based on barium-strontium niobate (BSN) films ($Ba_{0.5}Sr_{0.5}Nb_2O_5$ composition), PZT-ceramics and AFE-ceramics.

Material	P, μW	Petal size, mm	P_1, μW/mm²	V, volts
BSN films	500	3.5*0.5	7.14	50
PZT-ceramics	70	3.5*0.5	0.83	90
AFE- ceramics	1500	3.5*0.5	21.4	85

Table 1. A comparison of power of petal electrostatic micromotors on different materials.

Micromotor power can be increased by decreasing d down to 50-20 μm, or by increasing voltage pulse amplitude up to the breakdown voltage in the gap between the petal and the ferroelectric surface. According to estimates in (Dyatlov, et. al., 1996), this voltage can be as high as 200 V.
Besides, the power of the linear motor can be increased by increasing the operation clock frequency, the optimal value of which in turn depends on resonant frequency of the petal as have been shown above.
Thus the duration of the separation process does not affect the frequency properties of the motor, and clock frequency is limited by the duration of the electrostatic rolling process. The experimental clock frequencies for the ferroelectric films are in 10 – 20 kHz range (Dyatlov et al., 2000). Thus, the maximum specific power of the "ceramic" motor can be estimated to be equal to 100 – 300 μW/mm².

9. Some applications of the micromotors

High energy output allows one to obtain high absolute power (up to 0.01 – 1 W) increasing the rolling area, and therefore the described micromotors can be used in various MEMS devices, e.g., listed in Introduction.
Some applications of proposed micromotors in MEMS were analyzed by us both numerically and experimentally.
The possibility of creation of high speed (microsecond range) microcommutators powered by microactuator based on an electrostatic rolling of the thin metallic film on the ferroelectric film surface was considered in (Kostsov & Kolesnikov, 2007). The numerical analysis of the microcommutator operation was performed and its main characteristics were described. It was shown that the driving force developed by the microactuator in the first 10–100 μs of the electrostatic rolling is equal to 0.05–0.5 N per 1 mm of metallic film width, and the force is limited by the mechanical strength of the film. The high value of the force makes it possible to use strong springs that prevent the switchboard from switching between steady states even under the load factor of 1000 g and more
The research on opportunities of construction of high – efficiency micropumps and injectors of liquid microjets on the base of high energy-intensive electrostatic microactuators, working in a cyclic mode, was carried out (Kostsov & Sokolov, 2010). The design, the features of functioning, characteristic parameters of such devices are described. It is shown that a microactuator with the area of 1 mm² is capable to inject during one step with the duration of 30-300 μs a microjet of liquid with the weight of 1 - 3 micrograms, flowing out with the velocity of 1-10 m/s and more depending on the radius of exit nozzle.
Electrostatic high energy micromotor based on the ferroelectric films is studied as applied to microelectromechanical devices operating in vibrational mode (Baginsky et al., 2008). It is shown that the micromotor can be efficiently used in high frequency micromechanical vibrators that are used in high energy MEMS devices, such as micropumps, microvalves, microinjectors, adaptive microoptic devices etc.

The operation principle of micromechanical valve based on the effect of electrostatic rolling of metallic films on the ferroelectric surface was considered (Kostsov & Kamishlov, 2006). These microvalves differ from prototypes by high operation speed (microseconds), by ability to sustain a high pressures and by good fabricability.
Finally, the preliminary experiments and numerical modelling have shown that these microactuators can be used as microelectrogenerators with wide application range by reversing the described electromechanical energy conversion (Baginsky & Kostsov, 2002).

10. Results and discussion

The comparison of the operation parameters for the different types of the electrostatic micromotors is shown in table 2. Here $A_R = C_{sp}V^2/2$ is the electric work during one cycle. Mechanical work is $A_M = \eta A_R$. The energy conversion efficiency η value is determined by the micromotor construction. For the first two types of the micromotors relatively high efficiency values are achieved – up to 80%, for the micromotor described in this paper the efficiency can also be as high as 80% depending on the petal geometry. The analysis of the data in Table 2 shows the specific mechanical work of the described micromotors to be greater than A_M values typical for the known constructions of the micromotors used in MEMS by several orders of magnitude.

Micromotor type	d, μm	C_1, pF/mm²	V, Volts	A_R max. J/m²	A_R V=50 V J/m²	A_M V=50 V J/m²	A_M max. J/m²
Air gap	2-3	<4	0-50	10^{-2}	$5\ 10^{-3}$	$4\ 10^{-3}$	10^{-3}
Rolling on the linear dielectric	2-3	40	0-150	$5\ 10^{-2}$ –0.5	$5\ 10^{-2}$	$4\ 10^{-2}$	$4\ 10^{-1}$
Rolling on the ferroelectric	2-3	300-1000	20-200	5	1.3	1.05	1.25

Table 2. Comparison of the parameters of the different types of the electrostatic micromotors

This work shows that high energy output step reversible micromotors based on the ferroelectric layers can be created by micromachining for use in such MEMS where high specific power and operation speed are necessary.
These micromotors have the following advantages compared to the classical piezoelectric motors utilizing converse piezoelectric effect:

- higher unit step: 10 –20 μm per 1 mm of petal length rather than 1 μm per 1mm of ceramics length,
- longer range of slider motion: it is essentially equal to the length of the ferroelectric layer,
- microelectronic design and manufacturing,
- higher specific energy output (up to 100 W/kg) and driving force (up to 10^3- 10^4 N/kg),
- lower operating voltage necessary for the motion start,
- significantly lower hysteresis,
- flexible movement control, including reversible movement.

Studies of the reliability of the elements based on the bending effects in thin freely suspended films (which are used, for example, to form elements of dynamic diffraction gratings) showed that they have a high reliability, allowing for up to 5×10^{12} bending cycles without a significant change in the parameters (Trisnadi, 2004). The fatigue properties of bronze films have been well studied; their distinctive feature is the ability to withstand long-

term cyclic loads (more than 10^{12} cycles), provided that the sum of bending and tension stresses does not exceed the limiting fatigue stress (400—600 N/mm^2). In the problem under consideration, the electric strength of the ferroelectric film would not reduce the reliability of elements containing this film, because only a small part of the applied voltage drops on it. These micromotors can be used in MEMS devices in the following areas: step micro- and nanopositioners (one and two-dimensional), microoptics, adaptive optics, high-speed lightguide switches, microscanners, micropumps, e.g. for the inkjet cartridges, indicators, indicator panels, sensors, control and diagnostic systems, microgenerators of electric power, etc.

High energy output allows one to obtain high absolute power (up to 0.01 – 1 W) increasing the rolling area, and therefore the described micromotors can be used in macroscopic devices such as microair vehicles, microrobots, artificial muscles etc.

11. References

Akiyama T. & Fujita H. (1995). A quantitative analysis of scratch drive actuator using buckling motion. *Proceedings of Micro Electro Mechanical Systems, 1995, MEMS'95.IEEE,* pp.310-315. ISBN 0-7803-2503-6, Amsterdam, the Netherlands, 29 January-2 February 1995.

Antsigin V. D., Egorov V. M., Kostsov E. G. & Sterelychina L. N. (1985) Ferroelectric properties of thin strontium barium niobate films. *Ferroelectrics,* Vol. 63, No. 1, pp. 235-242, ISSN 0015-0193.

Baginsky I., Kostsov E. & Sobolev V. (2008). High energy microelecromechanical oscillator based on the electrostatic microactuator. Proc. SPIE, Vol. 7025, pp. E1-E8, ISSN 0277-786X.

Baginsky I.L. & Kostsov E.G. (2002). The possibility of creating a microelectronic electrostatic energy generator. *Optoelectronics, Instrumentation and Data Processing (Avtometriya.),* No.1, pp.89-102, ISSN 8756-6990.

Baginsky I.L. & Kostsov E.G. (2003). High-energy capacitance electrostatic micromotors. *J. Micromech. Microeng.*, Vol. 13, No. 2 , pp. 190 – 200, ISSN 0960-1317.

Baginsky I.L. & Kostsov E.G. (2004). Electrostatic micromotor based on ferroelectric ceramics. .J. Micromech. Microeng., Vol.14, No.11, pp. 1569- 1575, ISSN 0960-1317.

Baginsky I.L.& Kostsov E.G. (2007). High energy-density MEMS based on thin ferroelectric layers. *Ferroelectrics*, Vol. 351, No.1, pp. 69-78, ISSN 0015-0193.

Baginsky I.L.& Kostsov E.G. (2010). Reversible high-peed electrostatic "contact". *Semiconductors,* Vol. 44, No. 13, pp. 1654-1657. ISSN 1063-7826.

Burfoot J.C., & Taylor G.W. (1979). *Polar Dielectrics and Their Applications.* The Macmillian Press LTD, ISBN 0-520-03749-9, London – New Jersey.

Dyatlov V. L. & Kostsov E. G. (1998) Electromechanical energy converters of micromechanic devices on the basis of ferroelectric films. *Nuclear Inst. and Methods in Physics Research,* Vol. A 405 No. 2-3, pp. 511-513, ISSN 0168-9002.

Dyatlov V. L. & Kostsov E. G. (1999). High–effective electrostatic micromotors on the basis thin ferroelectric films. *Optoelectronics, Instrumentation and Data Processing (Avtometriya.),* No.3, pp 3-15, ISSN 8756-6990.

Dyatlov V. L., Kostsov E. G. & Baginsky I. L. (2000). High-effective electromechanical energy conversion on the basis of thin ferroelectric films. *Ferroelectrics* , Vol. 241, No.1, pp. 99 – 106, ISSN 0015-0193.

Dyatlov V.L, Konyashkin V.V., Potapov B.S. & Pyankov Yu.A. (1996). Planar electrostatic micromotors. *Electrical Technology* (Elsevier Sequoia), No. 1, pp. 1 – 18, ISSN 1028 – 7957.

Dyatlov V.L., Konyashkin V.V., Potapov B.S. & Pyankov Yu.A. (1991). *Film Electrostatics.* Nauka, ISBN 5-02-029683-X, Novosibirsk (in Russian).

Esashi M. & Ono T. (2005). From MEMS to nanomachine. *J. Phys. D: Appl. Phys,* Vol. 38, No. 13, pp.R223–R230, ISSN 0022-3727.

Harness T. & Syms R. R. A. (2000). Characteristic modes of electrostatic comb-drive X-Y microactuators. *J. Micromech. Microeng.,* Vol. 10, No. 1, pp. 7–14, ISSN 0960-1317.

Kim B.-H. & Chun K. (2001). Fabrication of an electrostatic track-following micro actuator for hard disk drives using SOI wafer. *J. Micromech. Microeng.,* Vol. 11, No. 1, pp.1–6, ISSN 0960-1317.

Kostsov E.G. & Kamishlov V.F. (2006). Microelectromechanical Micro-Valve. *J. nano and microsys. techn.*, N 12, pp. 57 -59, ISSN 1813-8586.

Kostsov E.G. & Kolesnikov A.A. (2007). Fast electrostatic microcommutators based on the ferroelectric films. *Ferroelectrics*, Vol. 351, No. 1, pp. 138-144, ISSN 0015-0193.

Kostsov E.G. & Malinovsky V.K. (1989). Large-scale use of ferroelectricity in microelectronics is reality. *Ferroelectrics,* Vol. 94, No. 4, pp. 457-462, ISSN 0015-0193.

Kostsov E.G. & Sokolov A.A. (2010). Microelectromechanical fuel injector for diesel engines. *Journal of nano and microsystem technique*, No 8, pp. 30 – 34, ISSN 1813-8586.

Kostsov E.G. (1995). Ferroelectric films: peculiarities in their application to construction of new generation of memory devices. *Ferroelectrics,* Vol. 167, No. 3-4, pp. 169-176, ISSN 0015-0193.

Kostsov E.G. (2005). Ferroelectric barium-strontium niobate films and multi-layer structures. *Ferroelectrics*, Vol. 314, No. 1, pp. 169-187, ISSN 0015-0193.

Kostsov E.G. (2008). Electromechanical energy conversion in the nanometer gaps. *Proc. of SPIE*, Vol. 7025, pp. G1-G8, ISSN 0277-786X.

Kostsov E.G. (2009). Status and prospects of micro- and nanoelectromechanics. *Optoelectronics, Instrumentation and Data Processing*, Vol. 45, No. 3, pp.189- 226,. ISSN 8756-6990.

Sato K. & Shikida M. (1992). Electrostatic film actuator with a large vertical displacement. *Proceedings of Micro Electro Mechanical Systems, 1992. MEMS'92. An Investigation of Micro Structures, Sensors, Actuators, Machines and Robot.IEEE,* ISBN 0-7803-0497-7, Travemunde , Germany, 4-7 February, 1992, pp. 1-5,.

Trisnadi J.I., Clinton B.C. & Monteverde R. Overview and applications of Grating Light Valve™ based optical write engines for high-speed digital imaging. (2004). *Proc. SPIE,* Vol. 5348, pp. 52-54, ISSN 0277-786X.

Wallrabe U., Bley P., Krevet B., Menz W. & Mohr J. (1994). Design rules and test of electrostatic micrimotors made by the LIGA process. *J. Micromech. Microeng.,* Vol. 4, No. 4, pp. 40–45, ISSN 0960-1317.

Yun B. H. (1973). Direct display of electron back tunneling in MNOS memory capacitor. *Appl.Phys.Lett.,* Vol. 23, No. 3, pp.152-153, ISSN 2158-3226.

Yun B. H. (1974). Measurements of charge propagation in Si_3N_4 films. *Appl. Phys. Lett.,* Vol. 25, No. 6, pp. 340- 342, 2158-3226.

Zappe S., Baltzer M., Kraus T. & Obermeler E. (1997). Electrostatically driven micro – actuators: FE analysis and fabrication. *J. Micromech. Microeng.,* Vol. 7, No. 3, pp.204-209, ISSN 0960-1317.

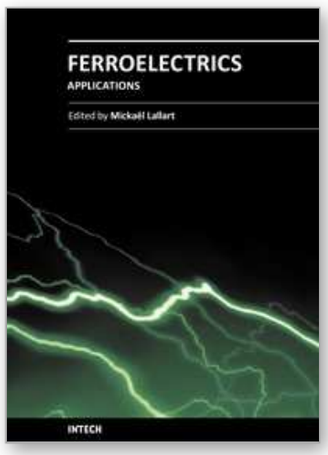

Ferroelectrics - Applications
Edited by Dr. MickaÃ«l Lallart

ISBN 978-953-307-456-6
Hard cover, 250 pages
Publisher InTech
Published online 23, August, 2011
Published in print edition August, 2011

Ferroelectric materials have been and still are widely used in many applications, that have moved from sonar towards breakthrough technologies such as memories or optical devices. This book is a part of a four volume collection (covering material aspects, physical effects, characterization and modeling, and applications) and focuses on the application of ferroelectric devices to innovative systems. In particular, the use of these materials as varying capacitors, gyroscope, acoustics sensors and actuators, microgenerators and memory devices will be exposed, providing an up-to-date review of recent scientific findings and recent advances in the field of ferroelectric devices.

InTech Europe
University Campus STeP Ri
Slavka Krautzeka 83/A
51000 Rijeka, Croatia
Phone: +385 (51) 770 447
Fax: +385 (51) 686 166
www.intechopen.com

InTech China
Unit 405, Office Block, Hotel Equatorial Shanghai
No.65, Yan An Road (West), Shanghai, 200040, China
中国上海市延安西路65号上海国际贵都大饭店办公楼405单元
Phone: +86-21-62489820
Fax: +86-21-62489821

IntechOpen